Autonomous Magnetic Navigation for Earth Orbiting Spacecraft

by Mark Psiaki, Cornell University
and Francois Martel, ITHACO, Inc.

1 Introduction

The strength and orientation of the Earth's magnetic field varies as a function of the location of the observations, which means that the magnetic field measurements contains position information.

Many artificial satellites carry a magnetometer on-board. The local magnetic field measurements could be used to provide navigation information. Such a navigation method has the advantage of requiring only data from low cost on-board instruments and has applications in low budget operation of satellite systems. Furthermore if processing can be performed on-board, this method leads to the possibility of fully autonomous long term navigation. In many systems magnetic navigation could be an effective back-up.

To study the feasibility and potential performance of spacecraft magnetic navigation, the concept was investigated using two possible approaches. In a first configuration the magnetic field orientation is assumed to be complemented by measurements of the Nadir direction provided by an Earth horizon sensor on board; the two vectors form the basis of a "space sextant." In the second configuration magnetic field magnitude is the sole source of external information.

2 Orbit Observability from Magnetometer Measurements

One type of position information is contained in the magnitude of the magnetic field. A simple dipole model of the Earth's magnetic field indicates that a given magnetic field magnitude corresponds to an ellipsoidal-type contour of possible S/C locations, as shown in Fig. 1. The figure's axis of rotational symmetry is along the magnetic dipole's axis (the horizontal axis of the figure). The basic information contained in the field magnitude is altitude-like information. The shape of the contour is such that no Keplerian orbit can remain on a single contour. This fact makes additional elements of the orbit observable through magnitude measurements. The geomagnetic field is not an exact dipole, and the
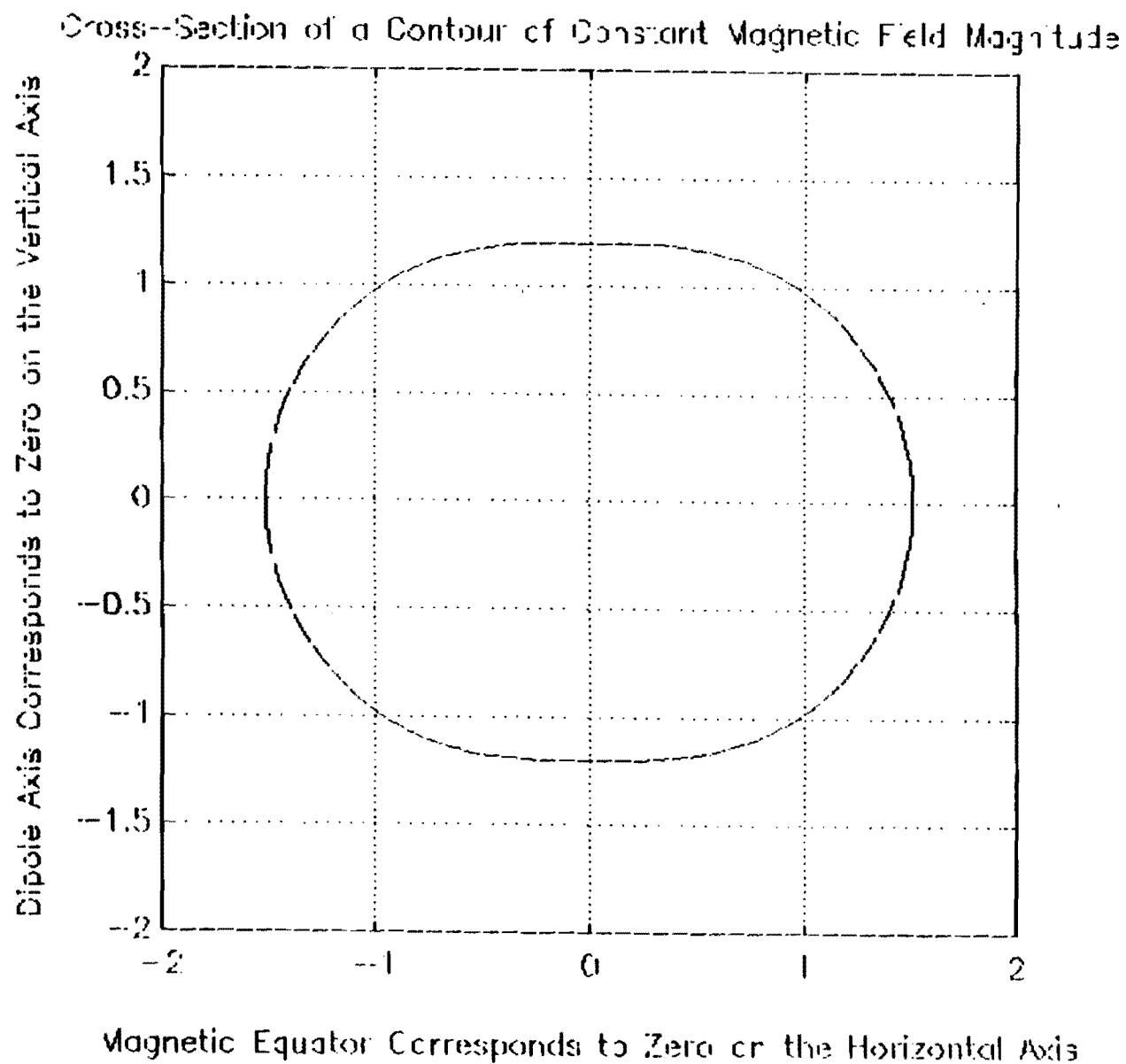
higher order terms "warp" this basic contour, and make Keplerian orbits even more observable from magnitude measurements.

If available, a nadir-vector measurement (from a horizon sensor) can give additional navigation information. The dot product of the nadir vector with the magnetic field unit vector, a quantity that can be computed independently of any estimation of the S/C attitude, gives the cosine of the angle between the nadir vector and the magnetic field vector. This type of computation is sometimes called an orbital sextant. The dipole model of the Earth's magnetic field again indicates the type of information contained in this angle. There is a one-to-one correspondence between this angle and the magnetic colatitude -- when this angle is 0° the S/C is at the magnetic north pole, 90° corresponds to the magnetic equator, and 180° corresponds to the magnetic south pole. Thus, the contour of constant cosine of this angle corresponds to a cone with its axis on the dipole axis.

The two measurements described above give two pieces of position information. A Keplerian orbit, however, has six elements as does a state-space description of the S/C state. The remaining information can be derived via filtering if the system is fully observable. For the case of magnitude measurements only, the question of observability has been partially addressed via linearization and the calculation of a 1-orbit observability Gramian. For a dipole model and a non-rotating Earth, the 1-orbit Gramian indicated that 5 of the 6 Keplerian elements are observable. The only unobservable element is the (Magnetic-) longitude of the ascending node. This is unobservable because of the rotational symmetry of the constant-magnitude contours (Fig. 1). The rest of the elements are observable because of the disparity between the shape of a Keplerian orbit and that of the contour; the magnitude of the magnetic field must vary during any orbit, and the signature of the variation serves to identify 5 of the 6 elements of the orbit. The addition of the orbital sextant information from the nadir measurement increases the observability of the 5 orbit elements that are already observable.

Longitude information is apparent in more complex models of the system. One source of longitude information is the rotation of the Earth coupled with the tilt of the Earth's magnetic poles. The rotation of the Earth causes the magnetic poles to change their tilt with respect to a fixed orbit, thus affecting the (Magnetic -) orbital inclination and other parameters that are observable. Another source of longitude information is the higher spherical harmonic content of the field. Effects such as the south Atlantic anomaly give longitude information on a daily basis. Instead of performing a more complex Gramian

Cross–Section of a Contour of Constant Magnetic Field Magnitude

Figure 1.

Dipole Axis Corresponds to Zero on the Vertical Axis

Magnetic Equator Corresponds to Zero on the Horizontal Axis

calculation to prove complete observability on a daily basis, observability has been demonstrated on a practical basis via state and covariance convergence in a filter simulation.

3 Filter Design and Theory of Operation

The basic filter used in this study is a Square Root Information Filter (SRIF) implementation of the extended Kalman Filter. It uses a nonlinear simulation of the orbital dynamics to propagate the state estimate and the linearized state transition matrix to propagate covariance information. It uses a linearized measurement information equation to update the state and covariance information. The state and the covariance are stored in the form of a linear square root information equation, and the propagation and updating schemes involve orthogonal upper-triangular (QR) factorization. A discussion of the SRIF can be found in Ref. 15. It is important to orbit determination problems because it reduces the effects of roundoff error on the covariance information. Having correct covariance information is critical to proper operation of sequential orbit estimators (filters) because they use the covariance to coordinate the estimation of 3-axis position based on a series of 1- or 2-axis measurements.

Several system modeling aspects are essential to proper filtering. A good model of the system's dynamics is necessary along with the mean and covariance statistics for any process noise that describes discrepancies between the dynamic model and the actual process. A measurement model is also needed for a filter. The measurement model must include the statistics of the measurement uncertainty's mean and covariance.

The dynamic model used for the current filter has 9 elements to the state vector (1). The first element is the inertial speed, V. The second element is the flight path angle, γ -- the angle between the inertial velocity and its projection into the local horizontal plane. The third element is the heading angle, ξ --the angle between local north and the projection of the inertial velocity vector into the local horizontal plane, measured positive for westward heading. The fourth element is the radial distance from Earth's center, r. The fifth element is the colatitude, θ. The sixth element is the east longitude, ϕ. The seventh through ninth elements are used to estimate the partially-nondimensionalized mean aerodynamic lift, drag, and side forces respectively, which are modeled as random walk processes. The actual quantities correspond to inverse ballistic coefficients, SC_L/m, SC_D/m, and SC_Y/m; S is a surface area, m is the S/C mass, and the C coefficients are nondimensional lift, drag, and side force coefficients respectively:

$$x = \begin{bmatrix} V \\ \gamma \\ \xi \\ r \\ \theta \\ \phi \\ SC_L/m \\ SC_D/m \\ SC_Y/m \end{bmatrix} \tag{1}$$

The equations of motion for the first six elements of the state vector are just Newton's laws and kinematics. The external forces include gravity (up to J2 effects) and aerodynamic forces. Part of the aerodynamic force is a function of the last three elements of the state vector and of the nominal atmospheric density. The other part of the aerodynamic force is a zero-mean, discrete time white noise forcing function. It is part of the modeled process noise. Its covariance has been sized based on typical diurnal atmospheric density variations and on typical S/C ballistic coefficients. The equations of motion for the last three elements of the state vector are simply discrete-time random walk models. The random inputs to these equations constitute the remainder of the modeled process noise. Each is a zero-mean, discrete-time white noise process with covariance size based on typical diurnal atmospheric density variations.

As stated in Section 2, the two measurements used by the filter are the field magnitude and the cosine of the angle between the field and nadir:

$$y = \begin{bmatrix} \sqrt{B_r^2 + B_\theta^2 + B_\phi^2} \\ \dfrac{-B_r}{\sqrt{B_r^2 + B_\theta^2 + B_\phi^2}} \end{bmatrix} \tag{2}$$

One version of the filter uses only the magnitude measurement, y_1. The other version uses both measurements. In the latter version, the nadir/field angle information is only used when this angle is between $11.5°$ and $168.5°$; at lesser or greater angles the measurement equation is too highly nonlinear for use in a standard extended Kalman filter implementation. The filter update algorithm compares the measurements with an 8-th order

4

IGRF magnetic field model. The measurement uncertainty is attributed totally to uncertainty in the field model, which is modeled as being altitude dependent and uncorrelated between the three axes (Ref. 16, p. 118). Additional uncertainty would be present due to the limitations of a magnetometer and due to the inaccuracy of the horizon sensor's measurement of the nadir vector. At around 0.1°, the latter source of uncertainty is negligible in comparison to the field model uncertainty. The magnetometer noise has been ignored for the following reason: the purpose of this preliminary study is to determine the quality of the navigation information intrinsic to the field model. Magnetometer implementations of commensurate sensitivity and accuracy, can then be selected to take optimuadvantage of it. The field model uncertainty is based on the assumption of a relatively quiet period with no magnetic storms. Degradation of the field model accuracy in times of geomagnetic storms may be the subject of a future study; note that the current filter does not take into account angular measurements around the geomagnetic poles (which are the potentially most turbulent areas) and therefore limits the possible effects of magnetic storms.

Two criteria have been used to evaluate each filter's performance. The first criterion is convergence of the filter state to the state of the simulated "truth model". This is an inductive demonstration of observability. The nominal system is neutrally stable; therefore, full-state convergence is improbable unless the system is observable. The second evaluation criterion is the steady-state level of the filter covariance. The process and measurement noise statistical models are fairly closely matched to the actual expected noise statistics. Therefore, each filter is near optimal, and the filter covariance gives a reasonable indication of the actual estimation accuracy. The covariance levels after filtering a day's worth of measurements give a good indication of the possible steady state accuracy of such a system.

Each test of the filter involves two stages. The first stage is to independently simulate a day's worth of orbiting, recording the state of the spacecraft, x, and the one or two measurements that the filter needs, y. The second stage is to perform a day's worth of filtering of the measurements resulting from the first stage, recording both the resulting state estimate and the resulting covariance. The state time history provided by the first stage provides the "truth" model for convergence evaluation of the state time history estimated in the second stage; the filter has the capacity to be started with any arbitrary state error. The covariance time history generated by the second stage indicates the filter's accuracy.

Because of time limitations, only two complete filter evaluation cases have been run. Both cases involve simulation of the same orbit. The initial conditions of that orbit correspond to[†]

Semi-Major Axis	7028.14	km
Eccentricity	.0498	
Inclination	50.0	deg
Longitude of the Ascending Node	90.0	deg
Argument of Perigee	0.0	deg
True Anomaly	45.0	deg
Lift Ballistic Coefficient	0.0	kg/m^2
Drag Ballistic Coefficient	50.0	kg/m^2
Side-Force Ballistic Coefficient	0.0	kg/m^2

The first test case filters both measurements, field magnitude and cosine of the angle between the field vector and the nadir vector. The second test case filters only the magnitude measurements.

The position convergence of the 2-measurement filter is demonstrated in Figs. 2-6. It converged from a total initial position error of more than 400 km to within 2 km after filtering 10,000 sec worth of data (less than two orbits). After 14 orbits (one day), the total position error converged to less than .33 km. Figures 2 and 3 give the same total position error information on different scales. Figures 4-6 give the components of the position error in local zenith-south-east coordinates. As expected, the longitudinal error (east error) takes the longest to converge. The radial error (altitude error) converges most quickly. The velocity states, the first three elements of x, converge about as quickly as the position states. The aerodynamic force coefficient states, the last three elements of x, take about the full day to converge, but the drag ballistic coefficient gets estimated fairly accurately after one day of filtering. These results are evidence that the system is completely observable.

Figures 7-11 give the same convergence information for the 1-measurement case (field magnitude only). Again, all states converge. The convergence is not quite as fast as for the 2-measurement case, and longitude error still lags behind the other position errors in

---

[†] J2 effects, Drag effects, and the Earth's rotation will cause most of these to vary in time.

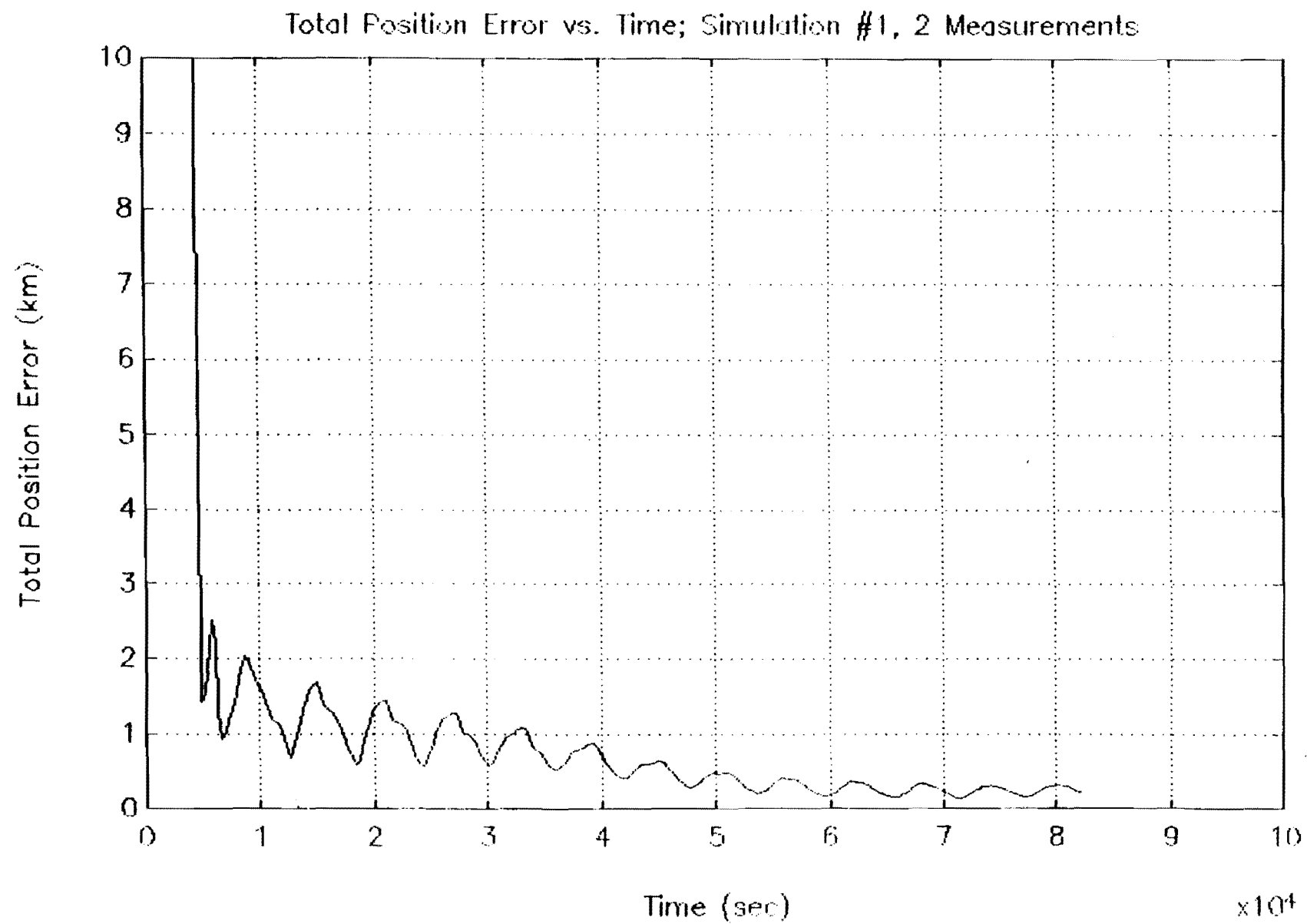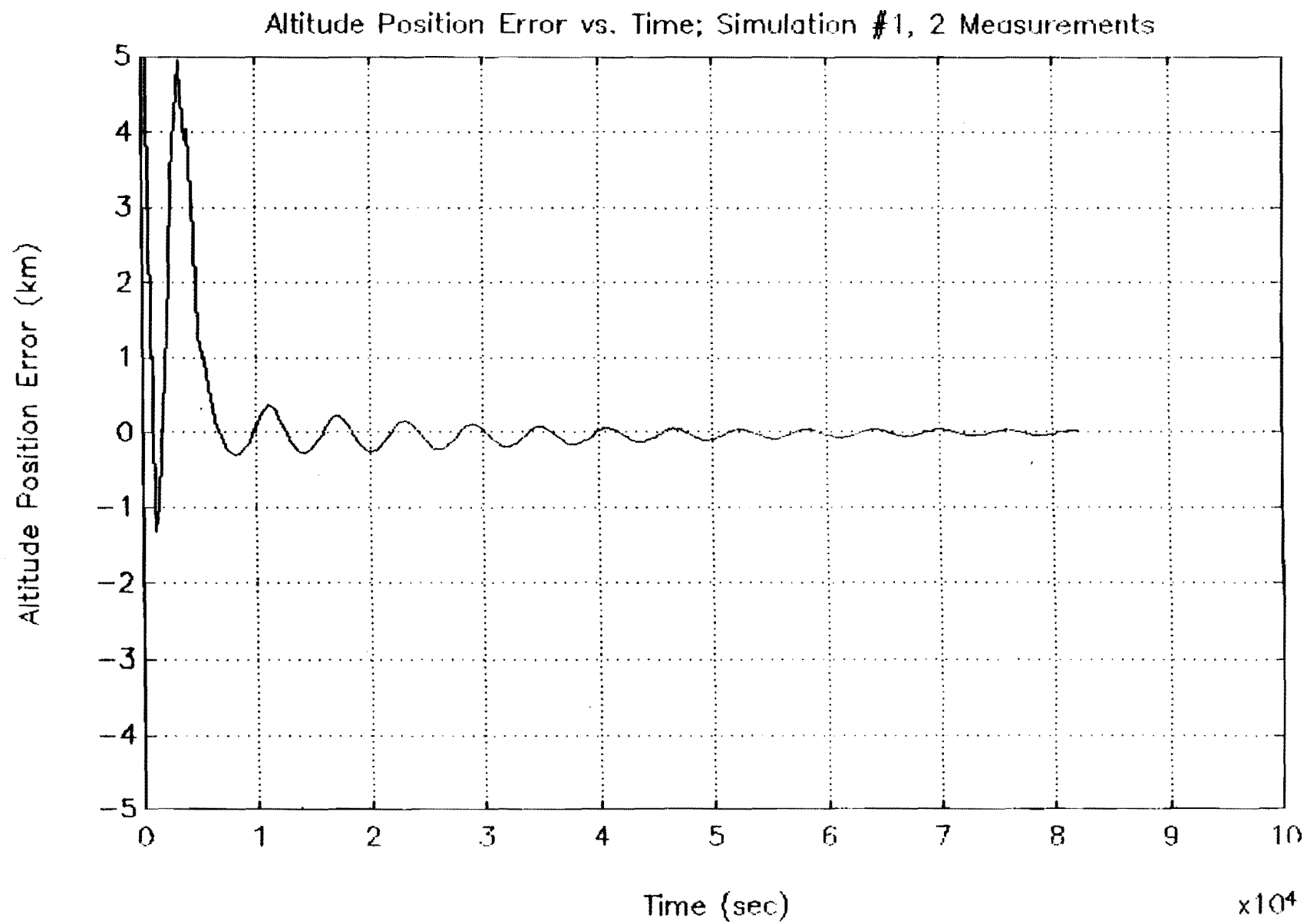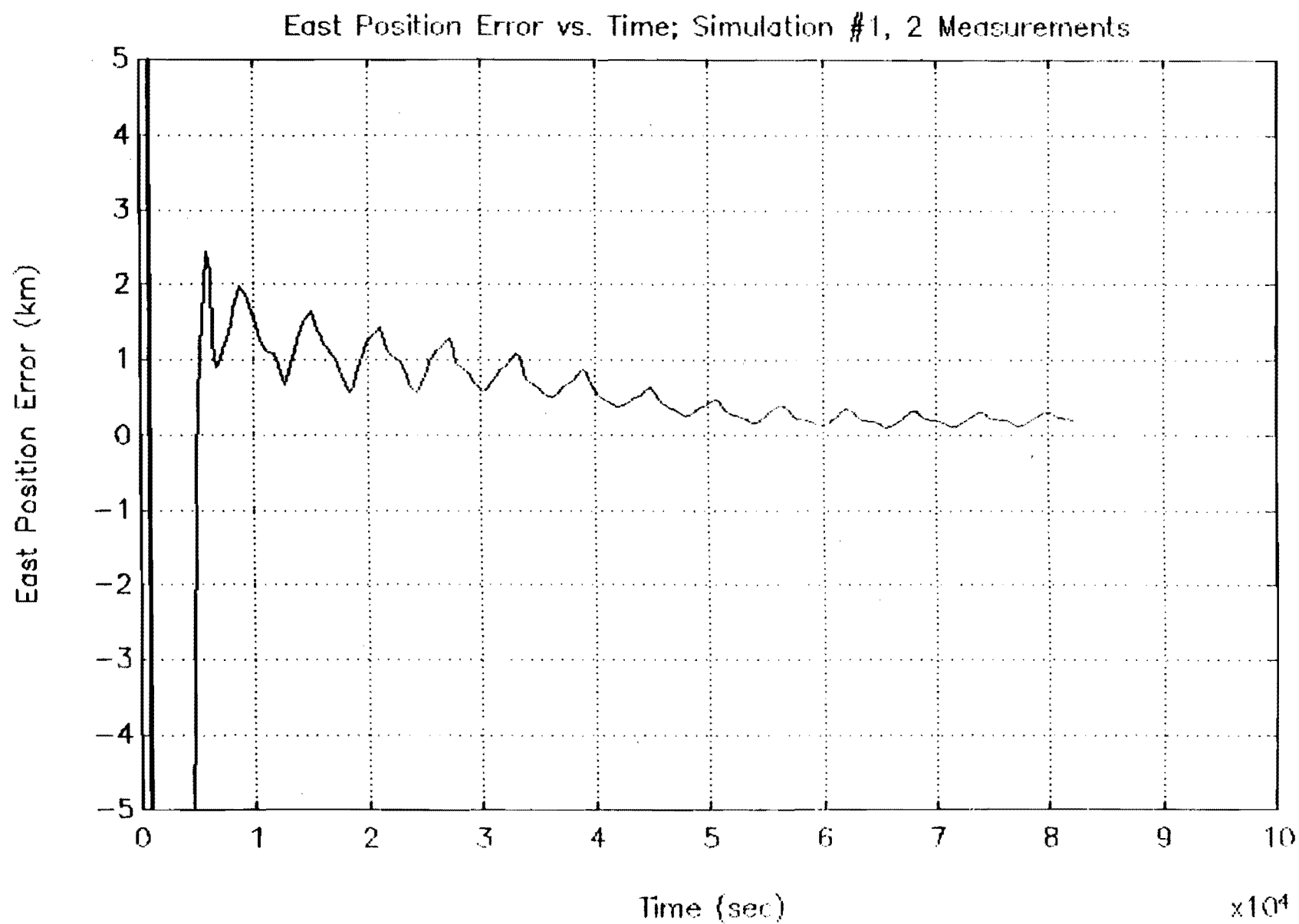Total Position Error vs. Time; Simulation #1, 2 Measurements

Figure 2.

Total Position Error (km)

Time (sec)

Total Position Error vs. Time; Simulation #1, 2 Measurements

Figure 3.

Altitude Position Error vs. Time; Simulation #1, 2 Measurements

Figure 4.

South Position Error vs. Time; Simulation #1, 2 Measurements
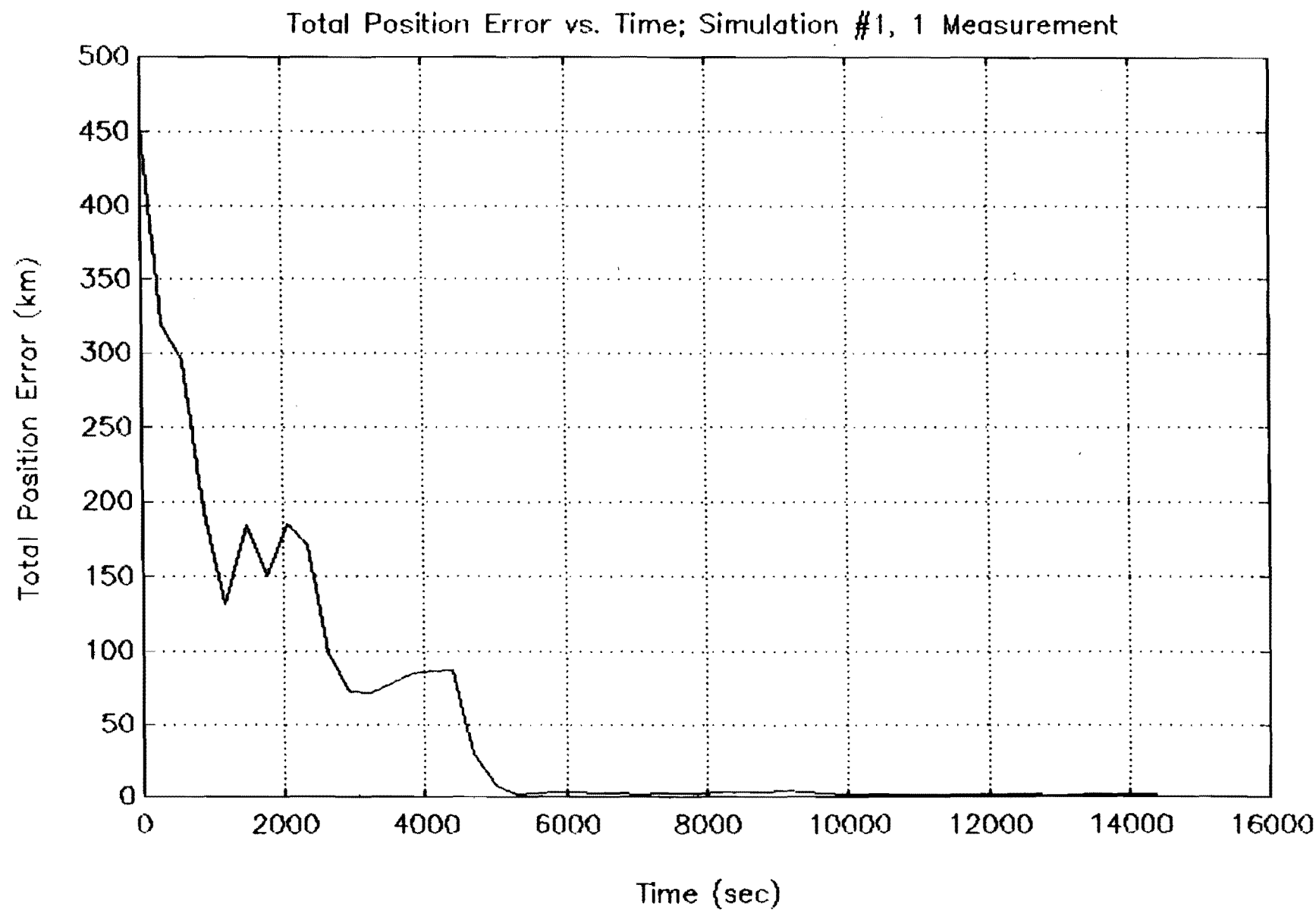
Figure 5.

East Position Error vs. Time; Simulation #1, 2 Measurements

Figure 6.

Total Position Error vs. Time; Simulation #1, 1 Measurement
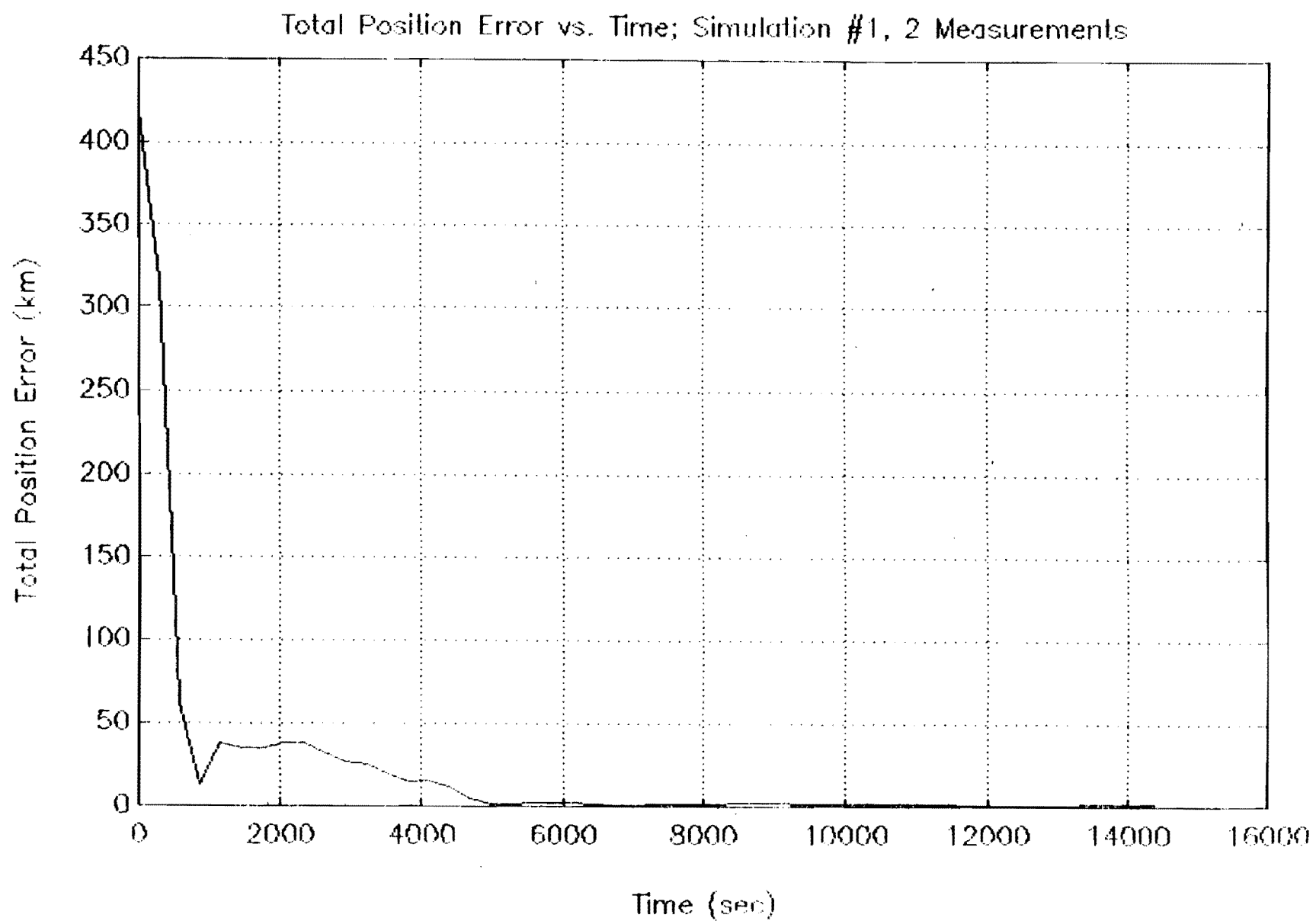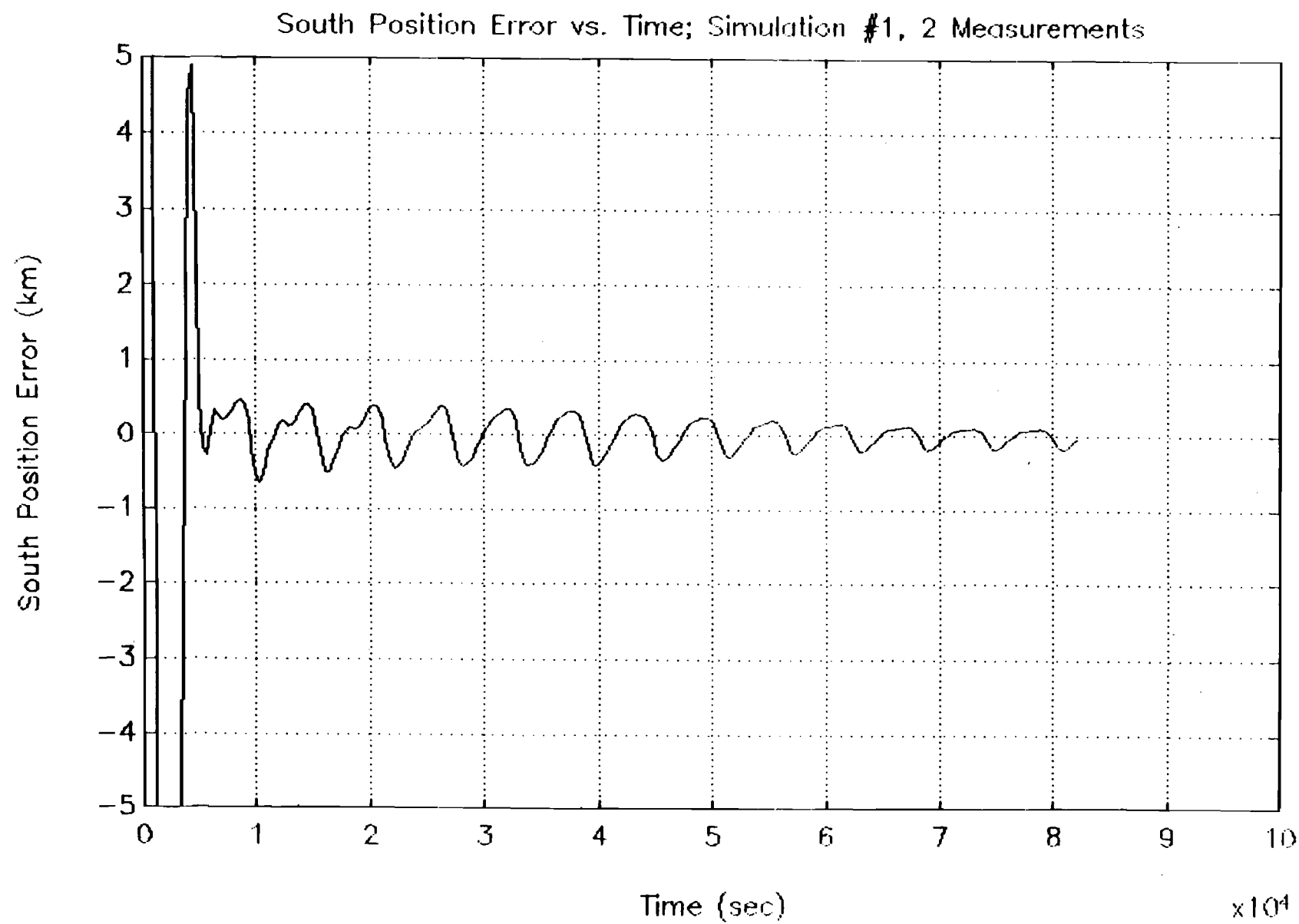
Figure 7.

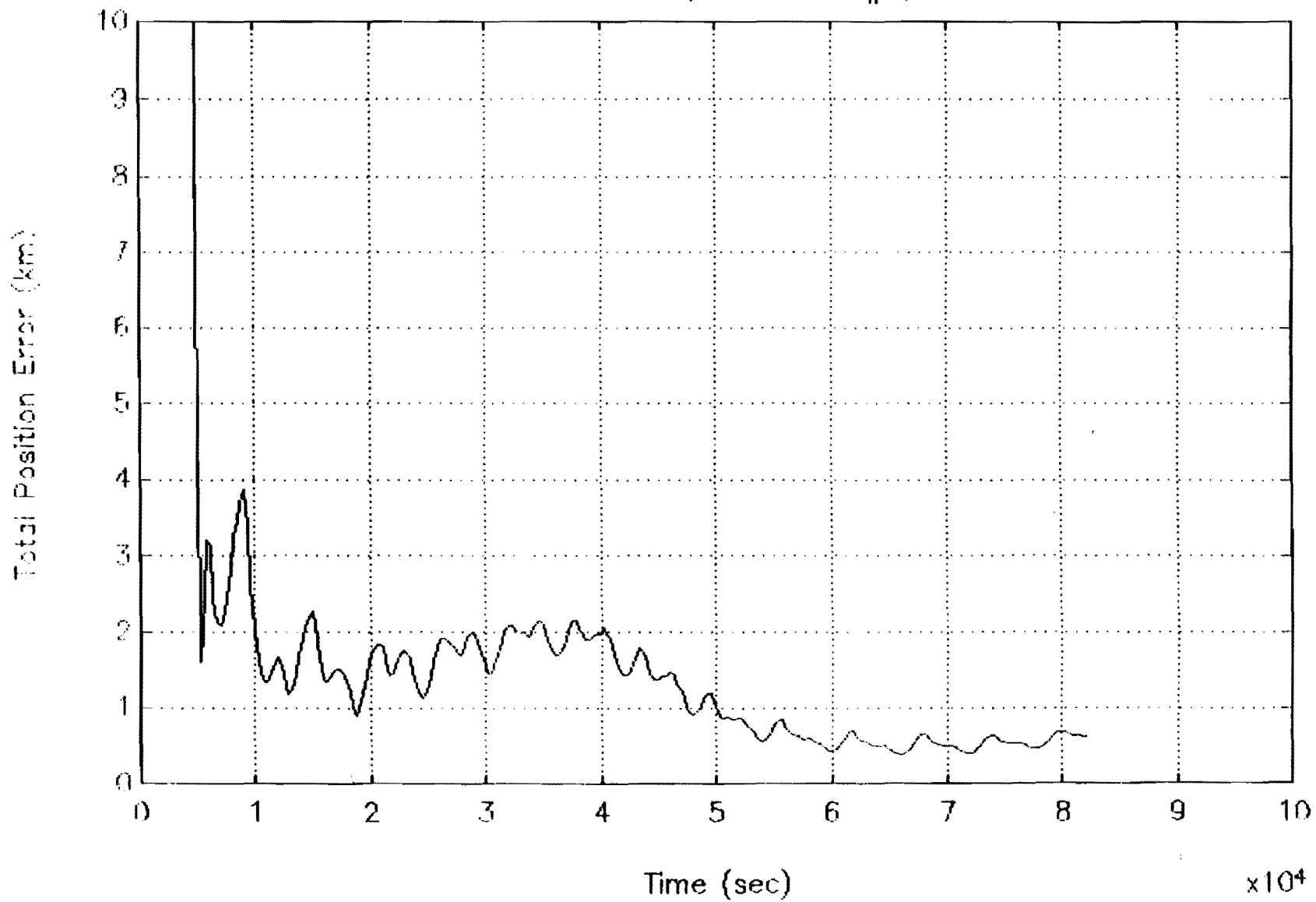Total Position Error vs. Time; Simulation #1, 1 Measurement

Time (sec)

Total Position Error (km)

Figure 8.

x10⁴

Figure 9.

Altitude Position Error vs. Time; Simulation #1, 1 Measurement

South Position Error vs. Time; Simulation #1, 1 Measurement

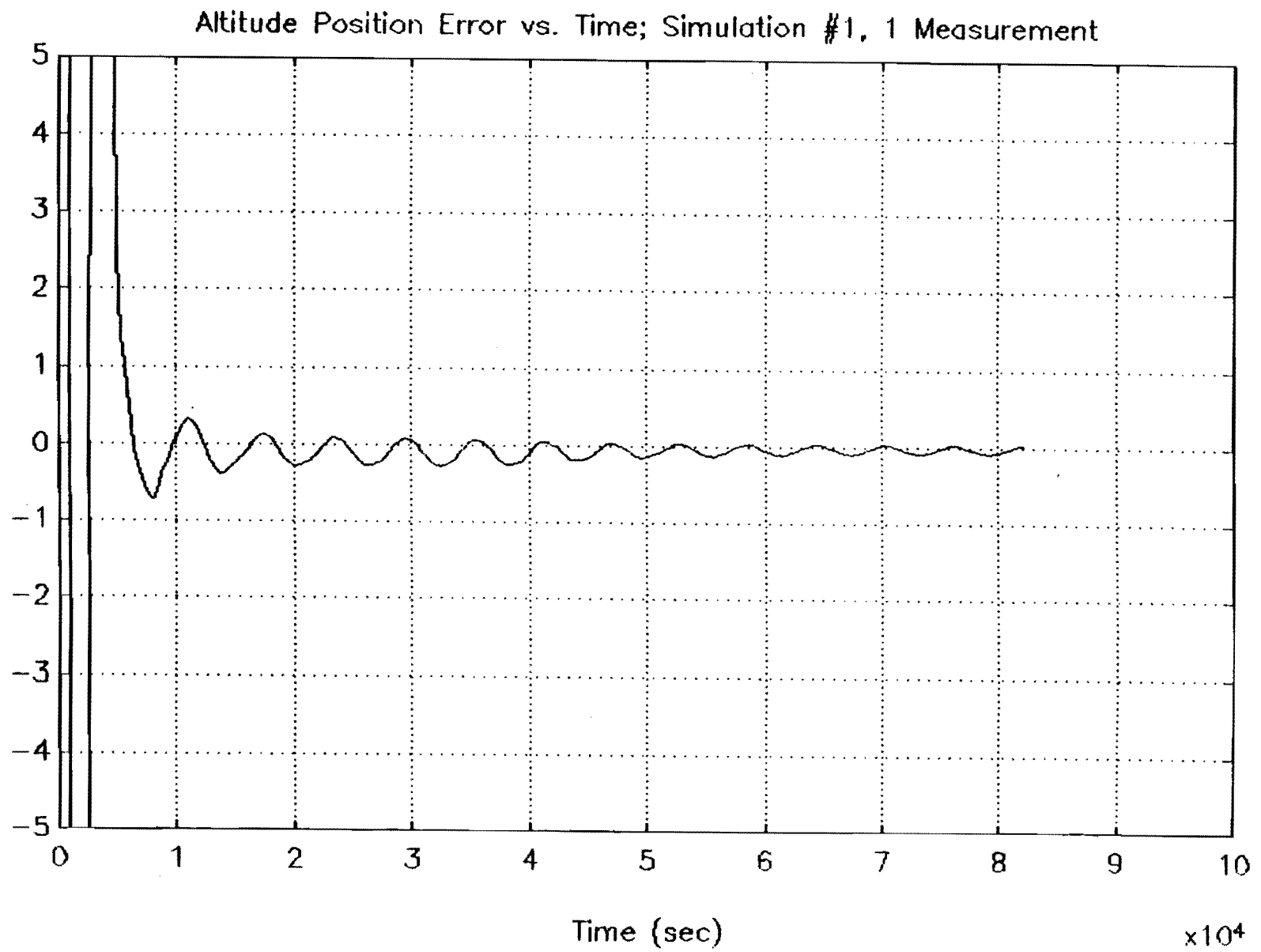Figure 10.

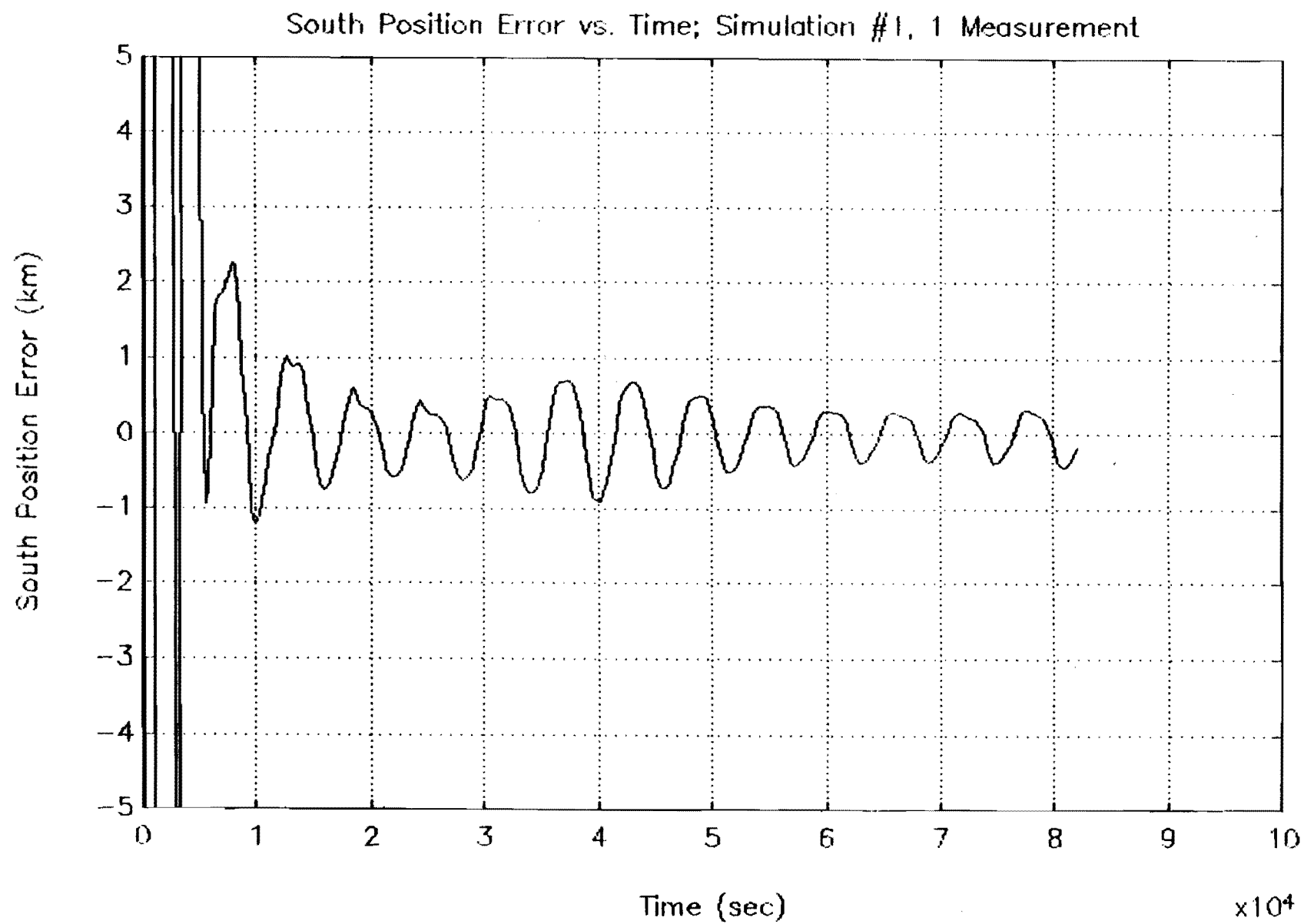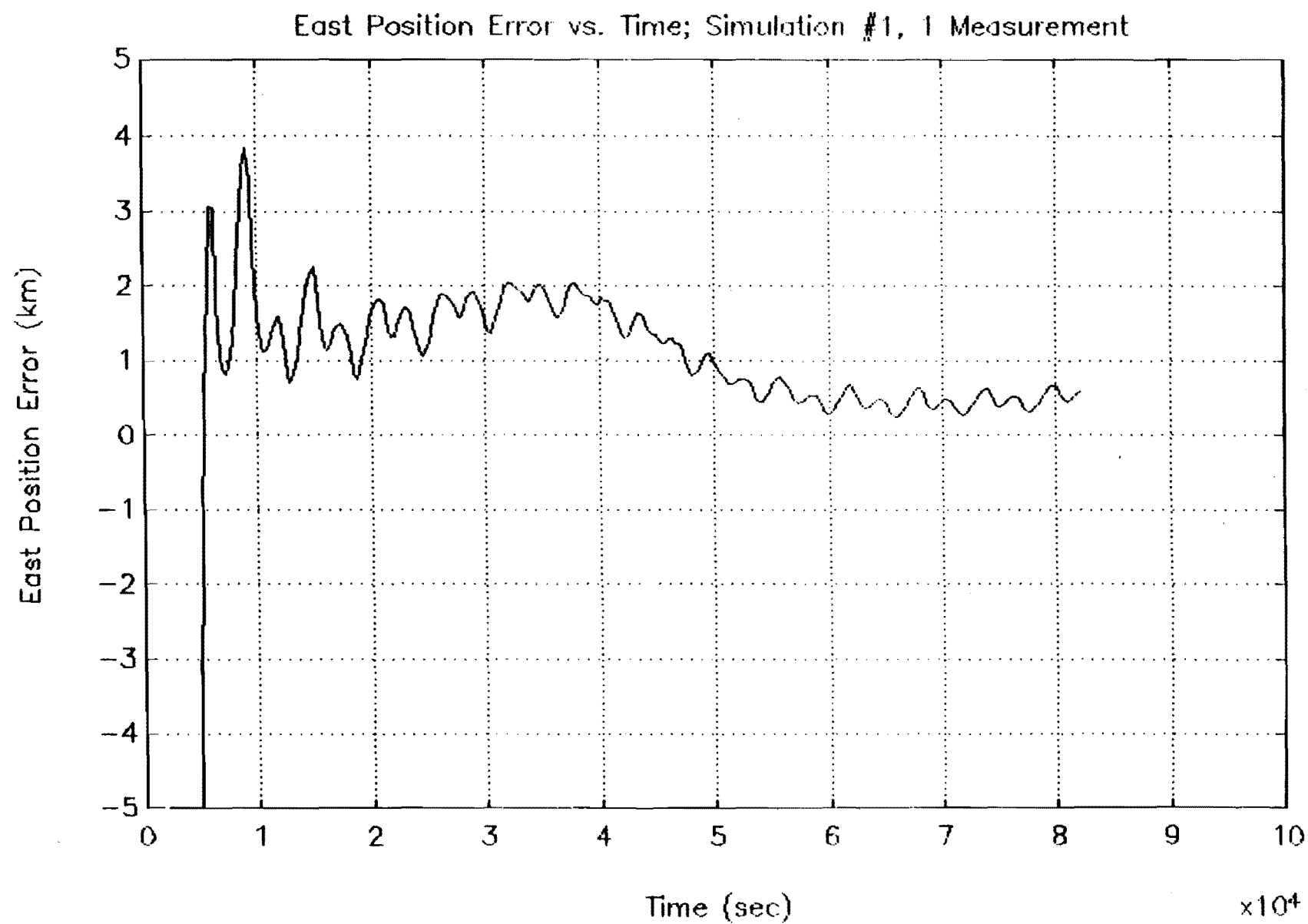East Position Error vs. Time; Simulation #1, 1 Measurement

Figure 11.

converging, but this result is still significant: total position error is reduced from 450 km to 2 km in about 2 orbits, and it continues to decrease throughout the day. Thus, the total orbital state seems to be observable from just the magnetic field magnitude measurement.

Figures 12-15 give the position standard deviations, σ, as functions of time for the two test cases. The three curves on each plot correspond to the three square roots of the three eigenvalues of the 3x3 position covariance matrix, which is a submatrix of the full 9x9 filter covariance matrix. Each curve has been labeled according to the dominant component of the eigenvector corresponding to the eigenvalue in question (e.g. the dotted curve is labeled east because longitude is the primary component that is varying with this standard deviation, though latitude is also a component). Figures 12 and 13 give the same three curves for the 2-measurement filter case. Figure 12 is plotted on a coarse vertical scale to show the convergence from large initial uncertainties, and Fig. 13 is plotted on a finer vertical scale to show the steady state performance. Figures 14 and 15 are the corresponding plots for the 1-measurement case (filtering of field magnitude only). These covariance results show that both filters have moderate accuracy even in the face of significant field model uncertainty. The 2-measurement filter achieves a steady-state 1-σ accuracy of .25 km in altitude, 1.5 km in latitude (south component), and 2.5 km in longitude (east component). The 1-measurement filter's 1-σ accuracy is comparable in altitude, but somewhat less accurate in the other two directions, 2.5 km in latitude, and 4 km in longitude.

6 Conclusions

This study has shown, in a preliminary way, the ability of a magnetometer-based system to perform navigation for an Earth-orbiting spacecraft. In conjunction with a horizon sensor and a computer implementation of a Square Root Information Filter, 3-axis position can be estimated to within a 1-σ accuracy of 2.5 km and better based on 24 hours worth of magnetometer data. Even without the horizon sensor, 1-σ accuracy of 4 km and better can still be achieved. These results are of a preliminary nature, being based only on a partial observability analysis and on two filter simulation cases. Also, the effects of magnetometer noise have been neglected. Nevertheless, a more thorough evaluation is likely to indicate a reduction of accuracy of no more than 50% as compared to the present results.

This method could provide a valuable, low-cost primary or back-up navigation capability. The magnetometer-only version of the system is especially attractive for back-
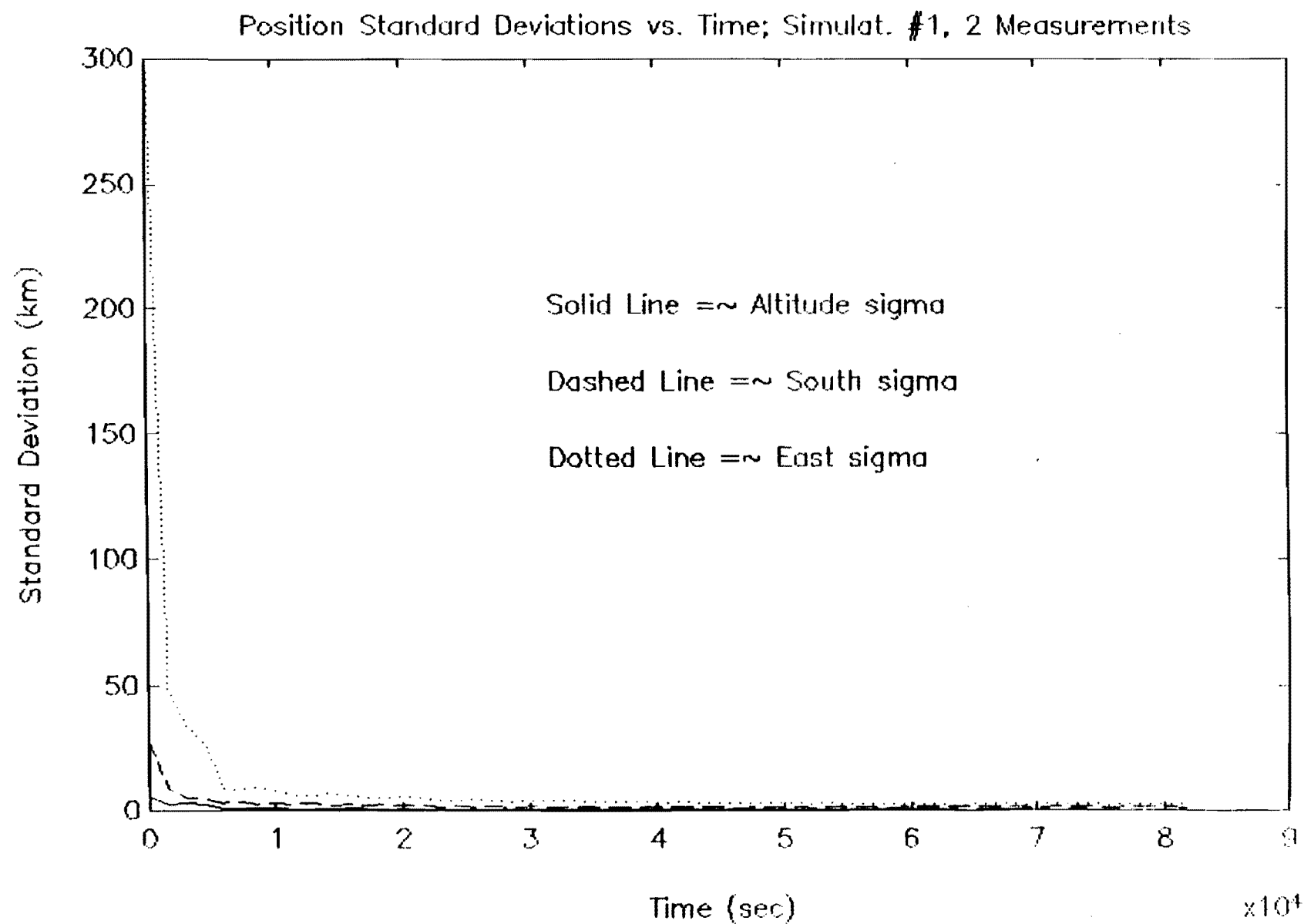
7

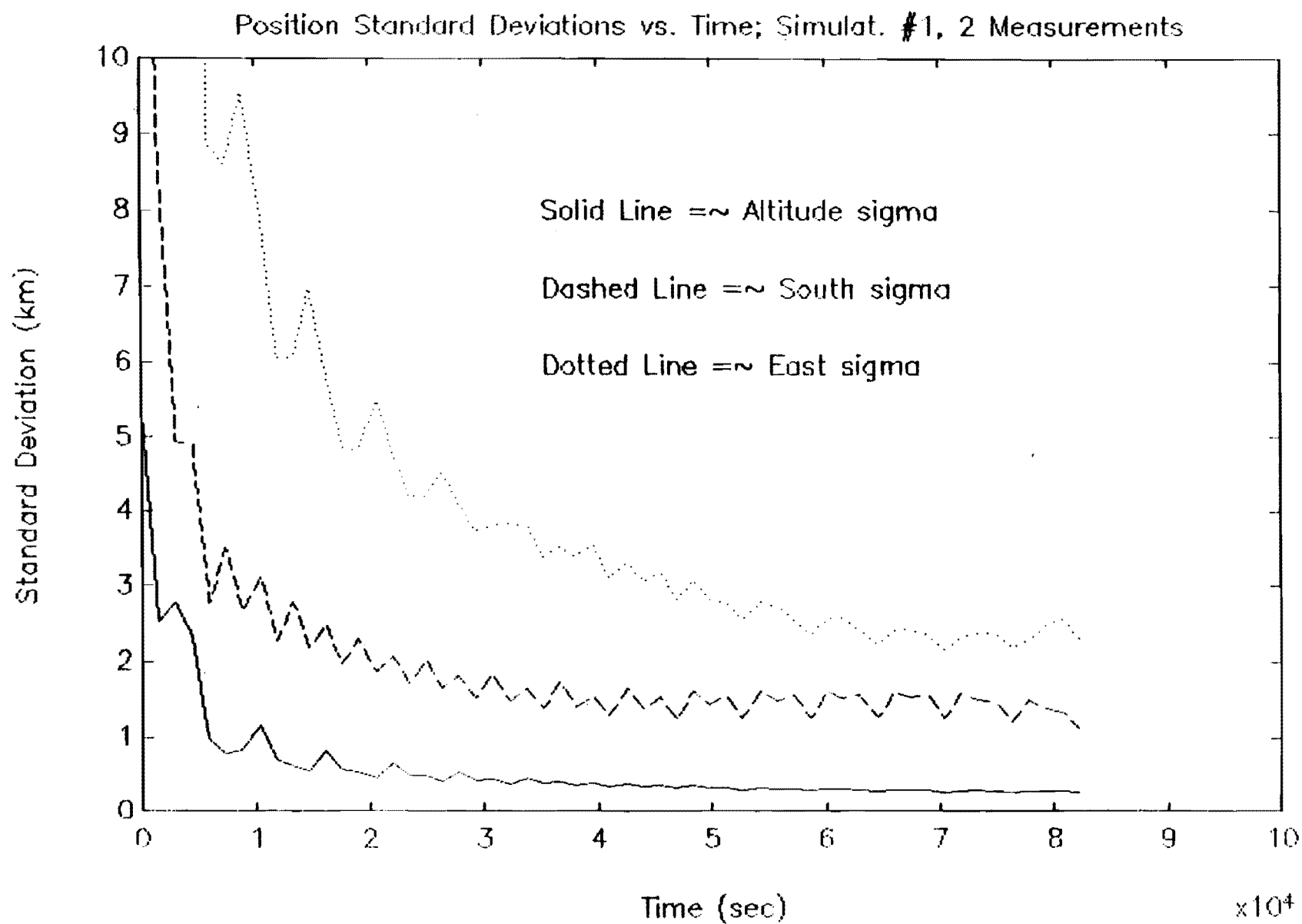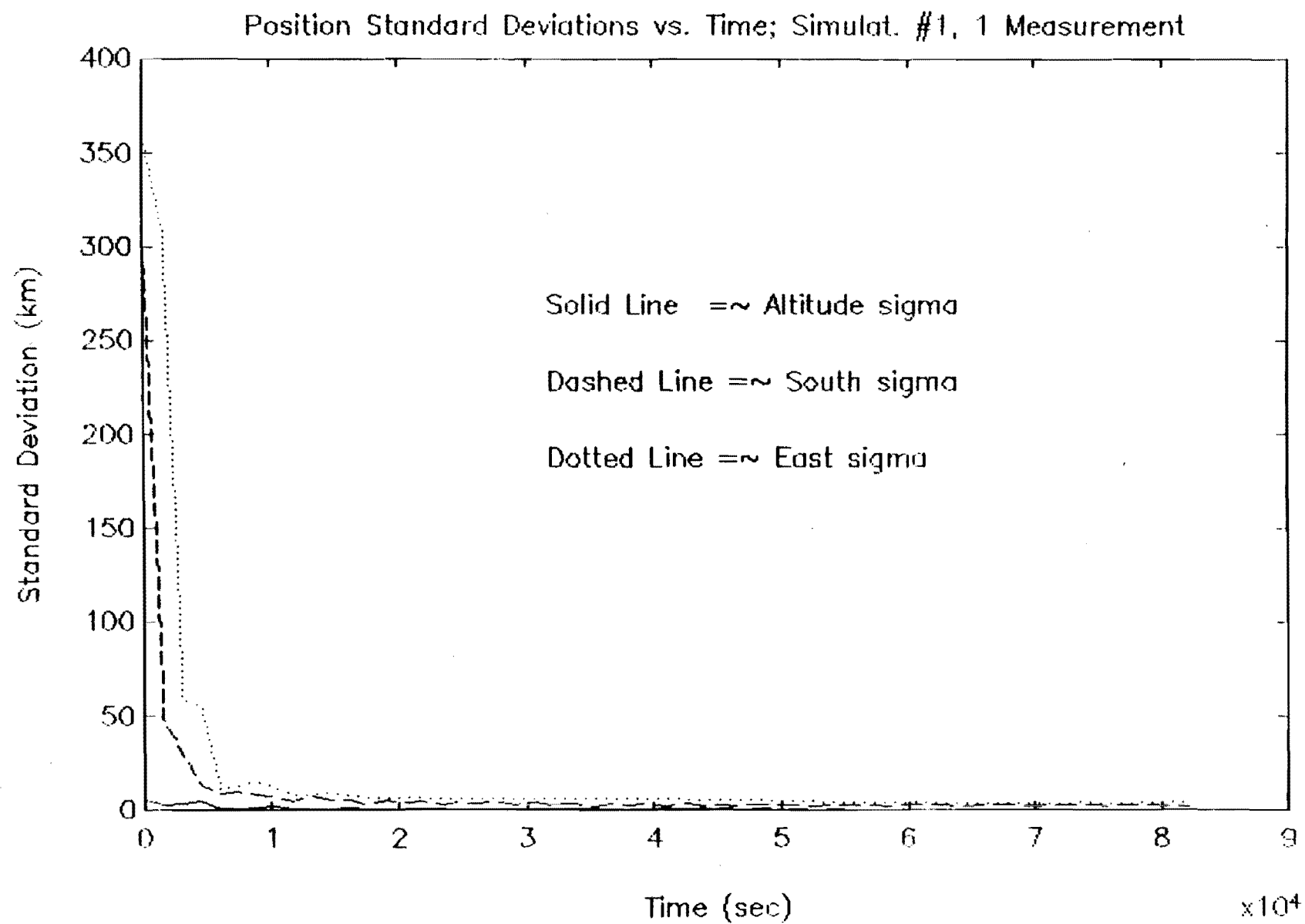Position Standard Deviations vs. Time; Simulat. #1, 2 Measurements

Solid Line =~ Altitude sigma

Dashed Line =~ South sigma

Dotted Line =~ East sigma

Standard Deviation (km)

Time (sec)

x10⁴

Figure 12.

Figure 13.

Position Standard Deviations vs. Time; Simulat. #1, 2 Measurements

Standard Deviation (km)

Time (sec)

x10⁴

Solid Line =~ Altitude sigma

Dashed Line =~ South sigma

Dotted Line =~ East sigma

Position Standard Deviations vs. Time; Simulat. #1, 1 Measurement

Solid Line =~ Altitude sigma

Dashed Line =~ South sigma

Dotted Line =~ East sigma

Standard Deviation (km)
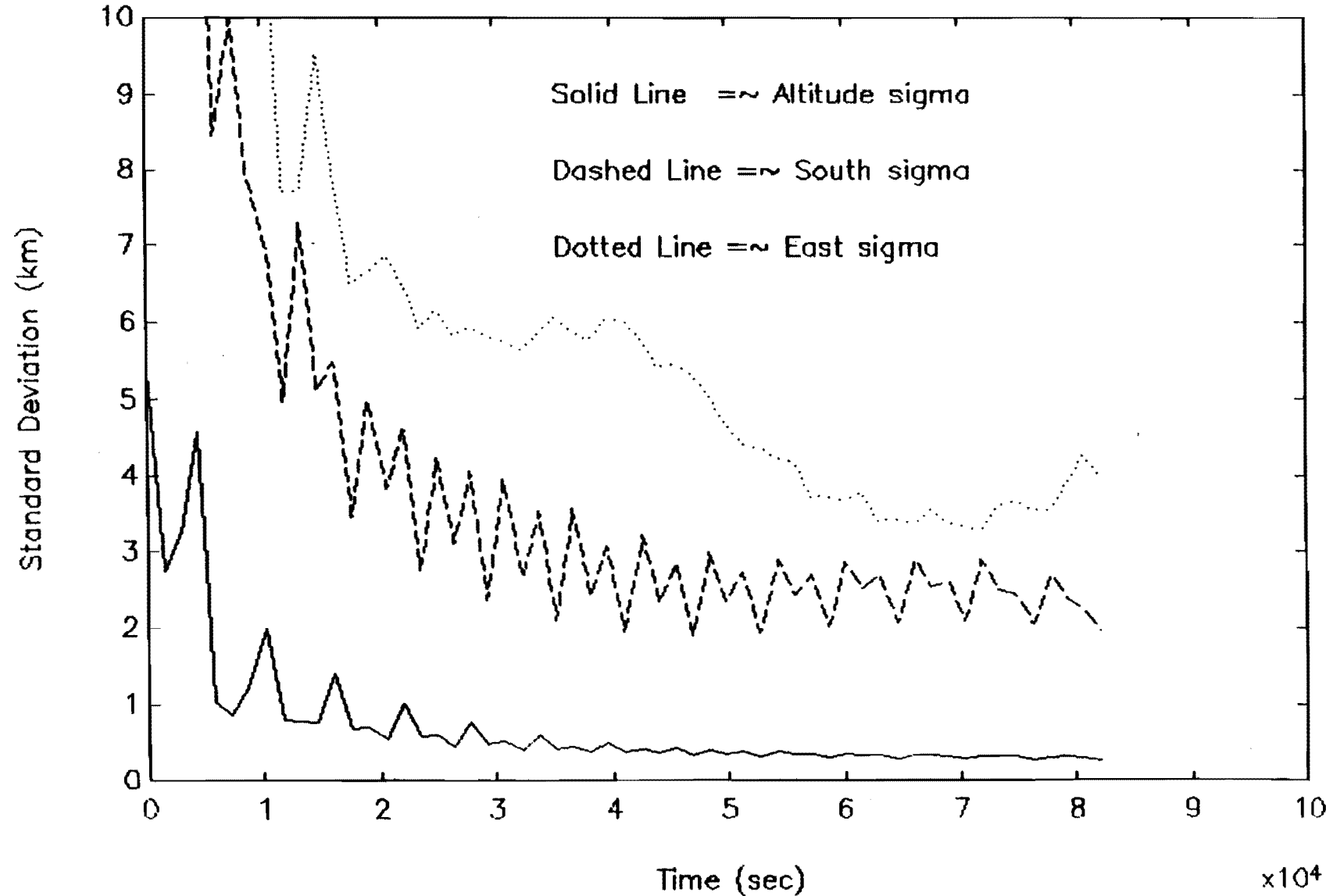
Time (sec)

x10⁴

Figure 14.

Figure 15.

up mode operation because it does not require any spacecraft attitude information. A simple microcomputer based ground station can perform the navigation filtering from magnetic field measurements transmitted from the spacecraft.

The square root information filter can be implemented in the flight computer to provide fully autonomous, continuous and long term navigation of the spacecraft, without any external interactions.

It must be noted too that, once the spacecraft position is known, the same magnetic field measurements can be filtered to provide the spacecraft attitude (ref 17). Magnetic field measurements can in effect be used for both autonomous navigation and attitude determination.

7 Bibliography

1. Chory, M.A., Hoffman, D.D., and LeMay, J.L., "Satellite Autonomous Navigation -- Status and History," Proceedings of the IEEE Position, Location, and Navigation Symposium, Las Vegas, NV, Nov. 4-7, 1986, pp. 110-121.

2. Fuchs, A.J., "Present and Future Trends in Near-Earth Satellite Orbit Determination," ESA Spacecraft Flight Dynamics, Aug. 1981, N82-14152, pp. 287-292.

3. White, R.L., and Gounley, R.B., "Satellite Autonomous Navigation with SHAD (Stellar Horizon Atmospheric Dispersion)," C.S. Draper Lab, April 1987, N88-13313.

4. Jackson, R.F. Jr., "Autonomous Navigation of USAF Spacecraft," Ph.D. Thesis, U. of Texas, Austin, 1983.

5. Ward, J.E., "Autonomous State Determination for an Earth-Orbiting Satellite using Horizon and Star Sensors," M.S. Thesis, Air Force Inst. of Tech., Wright-Patterson AFB, Ohio, Dec. 1984.

6. Eckstein, M.C., and Leibold, A., "Autonomous Station Keeping of Geostationary Satellites," in AGARD Spacecraft Pointing and Position Control, Nov. 1981, N82-20215.

7. Phillips, D., "Incorporation of Star Measurements for the Determination of Orbit and Attitude Parameters of a Geosynchronous Satellite: An Iterative Application of Linear Regression," Proceedings of the NASA GSFC Flight Mechanics/Estimation Theory Symposium, 1980, pp. 251-261.

8. Kan, S.P., "Autonomous Satellite Orbital Navigation and Attitude Determination," Proceedings of the NASA GSFC Flight Mechanics/Estimation Theory Symposium, 1978, pp. 178-193.

9. Ericson, N.L., Lundberg, J.B., and Tapley, B.D., "Autonomous Navigation using an Orbital Sextant Configuration -- A Near Earth Application," Proceedings of the AIAA/AAS Astrodynamics Conf., Aug. 15-17, 1988, Minneapolis, Minn., pp. 26-34.

10. Rychel, J.F., "The Sensitivity of an Autonomous Navigation Landmark Tracking System Due to the Variability of Landmark Availability and Distribution," Presented at the Institute of Navigation 42nd annual meeting, Seattle, Wash., 1986, A87-19367.

11. Vinokur, M.I., "Optimization of the Selection of Measurement Moments and Reference Stars for Navigation in the Problem of Autonomous Spacecraft Navigation According to Non-specified Reference Points," **Kosmicheskie Issledovaniia**, Vol. 24, Sept.-Oct. 1986, pp. 668-679. (in Russian)

12. Kulterer, G., "New Sensor Systems for Determining Spacecraft Position," Proceedings of the DGLR Annual Meeting, Oct. 8-10, 1986, Munich, W. Germany, pp. 46-57. (in German)

13. Lopes, R.V.F., and Kuga, H.K., "Optimal Estimation of Local Orbit from GPS Measurements," **Journal of Guidance, Control, and Dynamics**, Vol. 11, No. 2, March-April 1988, pp. 186-188.

14. Escobal, P.R., **Methods of Orbit Determination**, J. Wiley and Sons, (New York, 1965).

15. Bierman, G.J., **Factorization Methods for Discrete Sequential Estimation**, Academic Press, (New York, 1977).

16. Wertz, J.R. ed., **Spacecraft Attitude Determination and Control**, D. Reidel Pub. Co., (Boston, 1978).

17. M. Psiaki, F. Martel, P. Pal, **Three-Axis Attitude Determination via Kalman Filtering of Magnetometer Data**, Flight Mechanics/Estimation Theory Symposium, NASA/GSFC May 10-11, 1988